Proceeding Paper

A Computational and Spectroscopic Approach to Elucidate the Coordination Structures in Iron-Catechol Polymers †

Matías Capurso, Gabriel Radivoy, Fabiana Nador and Viviana Dorn *

Instituto de Química del Sur (INQUISUR-CONICET), Depto. de Química, Universidad Nacional del Sur, Av. Alem 1253, Bahía Blanca B8000CPB, Argentina; matias.capurso@uns.edu.ar (M.C.); gradivoy@criba.edu.ar (G.R.); fabiana.nador@uns.edu.ar (F.N.)

*   Correspondence: vdorn@uns.edu.ar
†   Presented at the 28th International Electronic Conference on Synthetic Organic Chemistry (ECSOC 2024), 15–30 November 2024; Available online: https://sciforum.net/event/ecsoc-28.

Abstract: Coordination polymer particles (CPPs) with catechol functionalities present significant potential for various applications. To elucidate their structural features, we synthesized CPPs using bidentate bis-catechol and catechol-pyridine ligands, and employed both computational and spectroscopic techniques. The results revealed distinct coordination environments: a four-center coordination for catechol-catechol and an octahedral coordination for catechol-pyridine. Experimental UV-Vis, IR and Raman spectroscopic analyses confirmed these findings, further supporting the accuracy of the computational model.

Keywords: coordination polymers; catechol; DFT; spectroscopy

1. Introduction

The use of catechol derivatives has garnered significant interest in the development of functional materials [1]. Catechols exhibit a remarkable ability to chelate various metals [2], making them ideal ligands for the generation of Coordination Polymer Particles (CPPs) [3]. These particles form through the self-assembly of metal ions and polydentate organic ligands in a poor solvent, which induces rapid precipitation (Figure 1). However, characterizing their final polymeric structure remains a significant challenge, partly due to their amorphous nature.

In this work, we present the use of two synthesized bidentate ligands bearing bis-catechol (ligand A) and catechol-pyridine (ligand B) functional groups in the preparation of CPPs through mixing with an Fe(III) salt (Figure 1). DFT calculations were performed using a simplified computational model to gain further insights into the structure of the coordination polymers and to support the characterization conducted with UV-Vis, IR, and Raman spectroscopies.
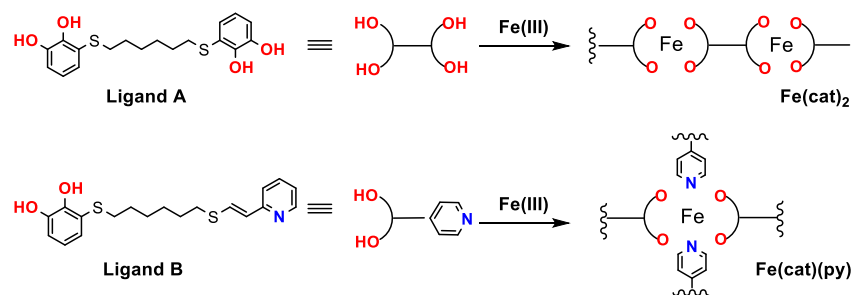
Figure 1. Formation of Coordination Polymer Particles (CPPs).

Chem. Proc. **2024**, *6*, x FOR PEER REVIEW

2 of 6

2. Methods

2.1. Polymer Preparation

The synthesis of CPPs involved dissolving the organic ligand in ethanol under magnetic stirring, followed by the dropwise addition of an aqueous $FeCl_3.6H_2O$ solution. Subsequently, a 0.1 M aqueous NaOH solution was added until a deep violet-blue color was achieved. The reaction mixture was stirred overnight, then subjected to centrifugation, washing with water and ethanol, and finally dried.

Experimental details for the synthesis of the ligands are reported in our previous work [4].

2.2. Spectra

UV-Vis spectra of CPPs were recorded on a Thermo Scientific™ ISA-220 with an Integrating Sphere Accessory in reflectance configuration. Spectra were collected over a wavelength range from 200 to 800 nm.

IR spectra were obtained using a Nicolet Nexus FT spectrophotometer in the range of 4000–400 cm^{-1} using an ATR module or KBr pellets.

For Raman spectra, a confocal Raman microscope was utilized with a 785 nm laser at 1% of the nominal potency (500 mW).

2.3. Calculations

All calculations were performed using the Gaussian 09 program [5]. Geometry optimizations of simplified CPP models were carried out using the BP-D3BJ [6,7] functional and the def2-TZVPP(Fe), TZVP(O, N), and SVP(C, H) basis sets [8] which have proven to be a reliable method for obtaining optimized geometries of iron-based complexes [9]. Frequency calculations were subsequently performed using the B3LYP-D3BJ [10,11] functional and the same basis set [8].

3. Results and Discussion

Based on the ultraviolet-visible (UV-Vis) spectra of the polymers, which exhibit an absorption maximum at 550 nm—a band corresponding to the metal-ligand charge transfer transition (MLCT) characteristic of the coordination of two catecholate ligands to an iron atom. Simplified molecular models were proposed to represent the structures of the coordination polymers, which we named $Fe(cat)_2$ and $Fe(cat)(py)$ (Figure 2). These structures were used for theoretical calculations of the respective infrared (IR) and Raman spectra. To assign the bands in the experimentally recorded spectra, we utilized the spectra of the free ligands A and B, as well as those simulated by DFT methods.
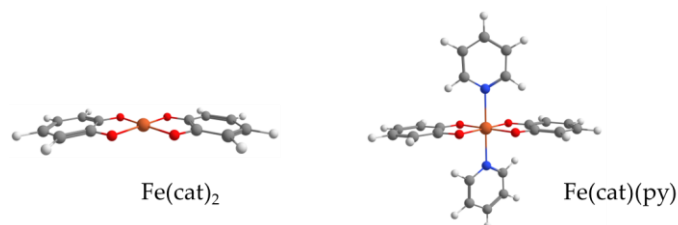

$Fe(cat)_2$ $Fe(cat)(py)$

Figure 2. Geometries of the structures used for theorical IR and Raman calculations.

Chem. Proc. **2024**, *6*, x FOR PEER REVIEW

3 of 6

3.1. IR Spectral Assigment

Region from 4000 to 2000 cm^{-1}

In this region, the O-H stretching band of the free catechol (A and B ligands), located around 3400 cm^{-1}, is no longer present in the spectra of the polymers. This observation corroborates the deprotonation of the hydroxyl group, which is necessary for coordination with the metal center. Furthermore, bands corresponding to the aromatic (~2950 cm^{-1}) and aliphatic (~2850 cm^{-1}) C-H stretching vibrations were identified, remaining practically unchanged upon polymer formation.

Region from 2000 to 1000 cm^{-1}

This region exhibits bands characteristic of aromatic ring vibrations and C-O bonds. Specifically, the bands at 1440 cm^{-1} and 1250 cm^{-1} correspond to C=C and C-O stretching modes, respectively, and are present in both the free ligands and the polymer samples. Conversely, the bands at 1330 cm^{-1} and 1150 cm^{-1}, associated with in-plane bending vibrations of the free catechol C-OH group, completely disappear in the polymer spectra, as expected.

Region from 1000 to 700 cm^{-1}

Three characteristic bands associated with C-H bending vibrations of the aromatic ring and aliphatic chain (C4 or longer) are observed. When comparing the spectra of the free ligands with those of the polymers, a slight shift of these bands to higher wav numbers is noted, from 890, 820, and 725 cm^{-1} to 920, 840, and 730 cm^{-1}, respectively. This shift is possibly due to the electronic effect of the metal on the electron density in the aromatic ring and the hydrocarbon chain.

Region from 700 to 400 cm^{-1}

Since the ATR crystal did not allow for spectral analysis in this low region of the IR spectra, it was necessary to prepare the samples using KBr pellets. The most relevant signal in this region corresponds to the Fe-O bond and is located at ~620 cm^{-1}. This signal is present in the polymers but absent in the free ligands, evidencing the coordination of the catecholate to the iron.
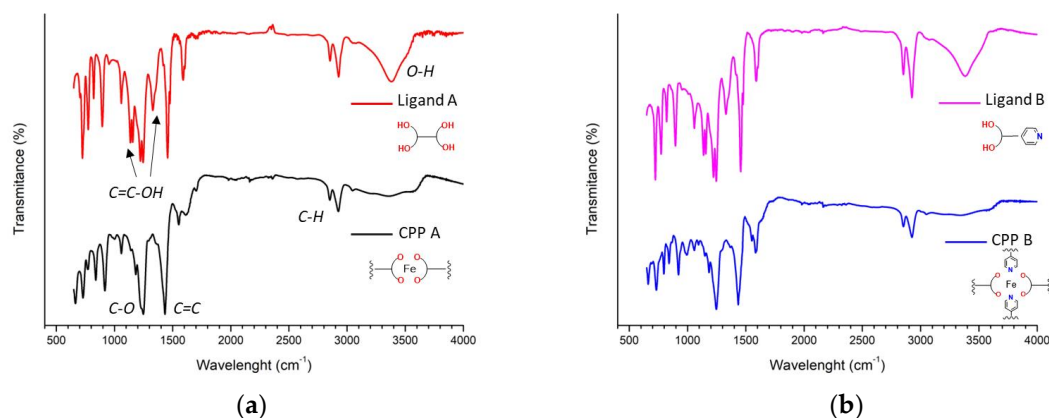

Figure 3. Infrared spectra of the ligands and their corresponding polymers.

Table 1. Main infrared frequencies (cm⁻¹) and assigments for the two systems.

Vibrations	υ =C-H	υ C-H *	υ C=C	υ C-O	Py Ring-brething	γ C-H	γ C-H	δ C-H *	Fe-O
Fe(cat)2 [DFT]	3101	-	1485	1254	-	956	871	-	608
CPP A [Exp]	2930	2855	1440	1250	-	920	840	730	626
Fe(cat)(py) [DFT]	3095	-	1475	1267	1042	945	869	-	643
CPP B [Exp]	2930	2855	1435	1250	1000	920	840	730	623

* These vibrations are not found in DFT modeling due to simplification of the structures.

3.2. Raman Spectral Assigment

Raman spectroscopy was employed to enhance the structural characterization of the polymers and, in particular, to identify the Fe-N coordination, which is essential for the formation of the polymeric Fe-(cat)(py) structure.

Region from 2000 to 1200 cm⁻¹

In this region, the characteristic bands of the vibrations of the aromatic ring and the =C-O bonds are found. In the case of the polymers, four signals are observed at 1560, 1450, 1330, and 1265 cm⁻¹. For the ligands, only one signal is observed around 1600 cm⁻¹. This could be due to the fact that the polymers are amorphous, which means they do not follow a symmetry pattern, leading to an increased number of observed bands.

Region from 1200 to 800 cm⁻¹

This region is of particular interest for the polymer containing the pyridine ring Fe(cat)(py), as the significant decrease in the intensity of the band at 1000 cm⁻¹ (Figure 4b), corresponding to the pyridine ring breathing mode, upon polymer formation serves as evidence of the coordination of the pyridine nitrogen to the metal.
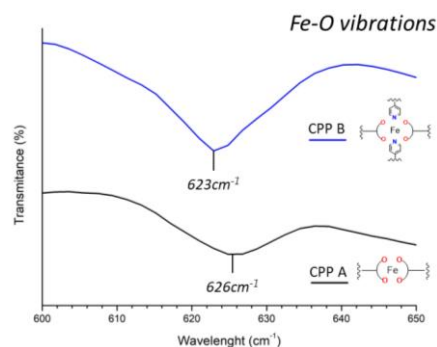

Figure 4. Fe-O vibrations on the infrared spectrum for both polymers.
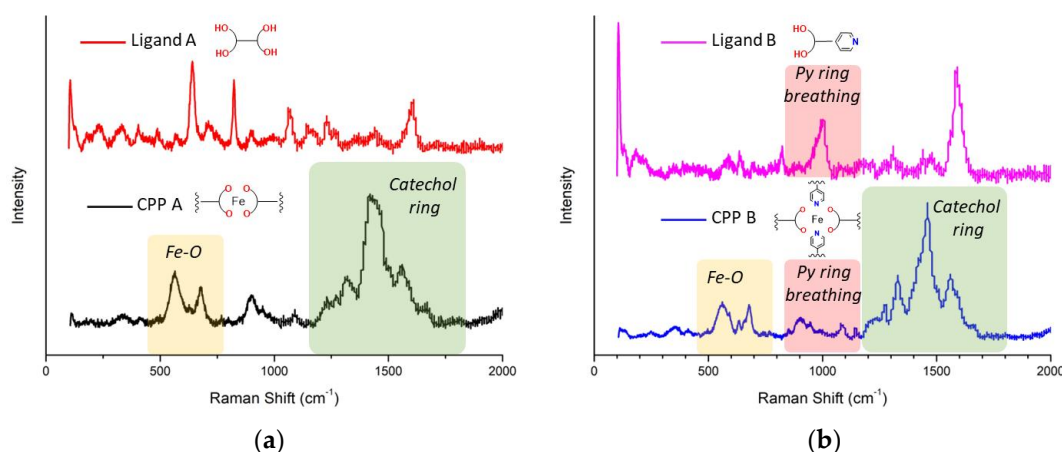
Figure 5. Raman spectra of the ligands and their corresponding polymers. (**a**) For ligand A; (**b**) For ligand B.

Region from 800 to 400 cm^{-1}

In this region of the Raman spectra, two distinct bands appear at 690 and 555 cm^{-1}, assigned to the Fe-O stretching vibration (marked with a yellow ring in Figure 4). These bands exhibit significantly higher intensity compared to the infrared spectra, providing compelling evidence for the formation of the Fe-O bond in the polymers. In contrast, the free ligands display a single band at 650 cm^{-1}, attributed to an OH bending mode of the catechol moiety, which disappears upon polymer formation.

4. Conclusions

The UV-Vis spectra revealed a characteristic absorption maximum at 550 nm, indicative of a bidentate coordination of two catecholate ligands to the iron center. DFT calculations were instrumental in interpreting the IR and Raman spectra, confirming the deprotonation of the catechol ligands, the formation of Fe-O bonds, and the coordination of the pyridine nitrogen. The agreement between the experimental and calculated spectra validates the proposed model, providing a foundation for future studies on analogous coordination polymer systems using fast and simple methods for their characterization.

References

1. Zhang, W.; Wang, R.; Sun, Z.; Zhu, X.; Zhao, Q.; Zhang, T.; Cholewinski, A.; Yang, F.; Zhao, B.; Pinnaratip, R.; et al. CatecholFunctionalized Hydrogels: Biomimetic Design, Adhesion Mechanism, and Biomedical Applications. *Chem. Soc. Rev.* **2020**, *49*, 433–464.

2. Saiz-Poseu, J.; Mancebo-Aracil, J.; Nador, F.; Busqué, F.; Ruiz-Molina, D. The Chemistry behind Catechol-Based Adhesion. *Angew. Chem. Int. Ed.* **2019**, *58*, 696–714.
3. Suárez-García, S.; Solórzano, R.; Novio, F.; Alibés, R.; Busqué, F.; Ruiz-Molina, D. Coordination Polymers Nanoparticles for Bioimaging. *Coord. Chem. Rev.* **2021**, *432*, 213716.
4. Nador, F.; Mancebo-Aracil, J.; Thiol-yne click reaction: An interesting way to derive thiol-provided catechols. *RSC Adv.* **2021**, *11*, 2074–2082.
5. Frisch, M.J.; Trucks, G.W.; Schlegel, H.B.; Scuseria, G.E.; Robb, M.A.; Cheeseman, J.R.; Scalmani, G.; Barone, V.; Mennucci, B.; Petersson, G.A.; et al. *Gaussian 09, Revision C.01*; Gaussian, Inc.: Wallingford, CT, USA, 2010.
6. Perdew, J. Density-functional approximation for the correlation energy of the inhomogeneous electron gas. *Phys. Rev. B* **1986**, *33*, 8822–8824.
7. Grimme, S.; Antony, J.; Ehrlich, S.; Krieg, H. A Consistent and Accurate Ab Initio Parametrization of Density Functional Dispersion Correction (DFT-D) for the 94 Elements H-Pu. *J. Chem. Phys.* **2010**, *132*, 154104.
8. Weigend, F.; Ahlrichs, R. Balanced Basis Sets of Split Valence, Triple Zeta Valence and Quadruple Zeta Valence Quality for H to Rn: Design and Assessment of Accuracy. *Phys. Chem. Chem. Phys.* **2005**, *7*, 3297.
9. Ye, S.; Neese, F. Accurate Modeling of Spin-State Energetics in Spin-Crossover Systems with Modern Density Functional Theory. *Inorg. Chem.* **2010**, *49*, 772–774.
10. Becke, D. Density-functional thermochemistry. III. The role of exact exchange. *J. Chem. Phys.* **1993**, *98*, 5648–5652.
11. Lee, C.; Yang, W.; Parr, R.G. Development of the Colle-Salvetti correlation-energy formula into a functional of the electron density. *Phys. Rev. B* **1988**, *37*, 785.